Physics and Chemistry of Minerals (2025) 52:19
https://doi.org/10.1007/s00269-025-01321-z

ORIGINAL PAPER

Experimental observations of $CaSiO_3$-$CaTiO_3$ perovskites: implications for Ca-rich inclusions observed in sub-lithospheric diamonds

A. R. Thomson[1,2,3] · W. A. Crichton[2] · N. C. Siersch[4] · I. S. Ezad[5] · D. P. Dobson[1] · J. P. Brodholt[1]

Received: 27 August 2024 / Accepted: 17 April 2025 / Published online: 4 May 2025

Abstract

Calcium perovskite is a major component of deep mantle phase assemblages and has been frequently identified, in retrograde form, as polyphase mineral inclusions within sub-lithospheric diamonds. Here experimental observations of synthetic samples demonstrate various properties of calcium perovskite minerals which have relevance for the interpretation of diamond-hosted inclusions. Ambient pressure diffraction and spectroscopy confirm the linear dependence of crystallographic unit cell volume and Raman peak shifts across the entire $CaSiO_3$-$CaTiO_3$ binary join. These systematics will allow verification of perovskite structure and constraint of inclusion composition, without destructive analyses, in future studies. Additionally, high pressure observations confirm that calcium perovskite minerals $\gtrsim$ 80 mol.% $CaSiO_3$ undergo spontaneous amorphization during decompression at room temperature, meaning they are unrecoverable. Finally, the presence of water appears to expand the calcium perovskite stability field to lower pressure conditions, implying at least some appreciable water-solubility in these minerals.

Keywords Calcium silicate perovskite · X-ray diffraction · Raman spectroscopy · Sublithospheric diamonds · Mantle mineralogy

Introduction

Calcium silicate perovskite (CaPv), whose $CaSiO_3$ endmember was recently named "davemaoite" (Tschauner et al. 2021), endmember is one of the major constituents of the Earth's deep mantle. After entering the phase assemblages of subducting mafic or ultramafic lithologies between 19 and 21 GPa (575–625 km depth) (Holland et al. 2013), except possibly at high temperatures (Ko et al. 2022; Muir et al. 2021), CaPv remains thermodynamically stable all the way to the core-mantle boundary (CMB). Throughout the lower mantle CaPv is believed to be the third most abundant mineral phase, after bridgmanite and ferropericlase, consisting up to ~5 wt.% of harzburgite, ~9 wt.% of pyrolite and ~31 wt.% of recycled basalt assemblages respectively (e.g. Kesson et al. 1998; Ricolleau et al. 2010, Stixrude et al. 2012). If Earth's mantle is assumed to be pyrolytic, possessing either a homogenous bulk composition or one that is composed of a mechanical mixture of basalt and harzburgite, CaPv will be the fourth or fifth most volumetrically abundant oxide mineral in our planet (Stixrude et al. 2012), of approximately equal overall abundance to garnet. CaPv is, therefore, undeniably a significant contributor to the chemical, geodynamic and geophysical behaviour of the Earth's deep mantle.

Providing verification of its presumed abundance throughout the mantle are multiple reports of former CaPv minerals occurring as inclusions trapped within sub-lithospheric diamonds (Brenker et al. 2007, Harte et al. 1994; 1999, Zedgenizov et al. 2014, Hayman et al. 2005, Kaminsky et al. 2001, Joswig et al. 1999, Thomson et al. 2014, Bulanova et al. 2010, Walter et al. 2008, Walter et al. 2011, Burnham et al. 2015, Zedgenizov et al. 2016, Anzolini et al. 2016, Anzolini et al. 2018, Smith et al. 2018, Stachel et al. 2000, Brenker et al. 2005, Davies et al. 2004, Tappert et al.

✉ A. R. Thomson
a.r.thomson@ucl.ac.uk

1 Department of Earth Sciences, University College London, London, UK

2 European Synchrotron Radiation Facility, Grenoble, France

3 Department of Earth Sciences, Natural History Museum, London, UK

4 Stuttgart, Germany

5 School of Earth Sciences, The University of Western Australia, Perth, Australia

2005, Korolev et al. 2018, Nestola et al. 2018). These samples predominantly have compositions, excluding a few wt.% of additional oxide components, falling within the $CaSiO_3$-$CaTiO_3$ system. With only two reported exceptions, none now possess their presumed primary perovskite crystal structure. Instead, they all consist of low-pressure assemblages believed to have formed during retrograde reactions that occurred on their way to the surface. Their interpretation as former CaPv minerals has been justified by (i) the ABO_3 stoichiometry of their bulk compositions and (ii) their current mineralogies match phases expected to form during CaPv retrogression (Joswig et al. 1999; Kubo et al. 1997). Thus, despite not retaining their presumed original perovskite structures, these samples have been used to provide insights into deep mantle processes. In particular, their high enrichment in trace elements and heavy oxygen isotopic compositions has been inferred to directly link these inclusions, and the diamonds that carry them, to the deep recycling and melting of subducted oceanic crust at transition zone depths (Stachel et al. 2000; Walter et al. 2011, 2008; Bulanova et al. 2010; Thomson et al. 2014; Burnham et al. 2015). Any such inferences clearly rely on the fidelity of interpretations that these inclusions are indeed retrograde products of former perovskite, and not simply "low"-pressure samples as has recently been suggested for some samples (Woodland et al. 2020).

It is apparent that, better than studying retrogressed inclusions, would be to identify and investigate inclusions of pristine CaPv; ones that retain their high-pressure crystal structure. Any such sample, e.g. those reported by Nestola et al. (2018) or Tschauner et al. (2021), would not only provide incontrovertible proof of their deep mantle origin but also permit direct investigation of deep mantle properties without requiring consideration of any effects of retrogressive re-equilibration. Unfortunately, due to results presented in this study and based on arguments of Walter et al. (2022), it appears that neither of these reports were recovered CaPv (of close to $CaSiO_3$ composition). However, verification of these samples as pristine $CaSiO_3$ perovskite has been hampered because the appropriate experimental, crystallographic and spectroscopic data required for the identification of primary, non-retrogressed, $CaSiO_3$-$CaTiO_3$ perovskite minerals were sparse to non-existent. Here we present Raman spectroscopy and X-ray diffraction observations from synthetic CaPv samples that rectify this gap in existing knowledge. Additionally, we present new experimental observations that constrain both the low-pressure extent of the CaPv stability field, with and without the presence of H_2O. These data will facilitate insight into diamond-hosted CaPv inclusions in future studies.

Methods

The data presented and discussed in this study originate from experiments performed at beamline ID06-LVP of the ESRF. Whilst some of the experiments were performed to directly investigate the stability of CaPv, others primarily investigated acoustic velocity of CaPv samples at mantle *PT* conditions. A subset of these ultrasonic experiments have previously been described (Thomson et al. 2019); specifically the room temperature decompression data of $CaSiO_3$ is already reported in supplementary information Table 4 of Thomson et al. (2019). With this exception, all data and refinements from these experiments are presented here for the first time. As there are multiple materials and measurements reported in this study, to try and avoid confusion these are summarised in Table 1 as well as being described below.

Starting materials

Starting materials with compositions $Ca[Si_xTi_{1-x}]O_3$ ($x = 0$, $0.56 \leq x \leq 0.8$ and $x = 1$) were created by weighing and grinding high purity SiO_2, $CaCO_3$ and TiO_2 in an agate mortar until they were fine homogenous powders. All compositions were decarbonated via ramped heating to 1000 °C in air. Intermediate bulk compositions ($0.56 \leq x \leq 0.8$) were fused using a one-atmosphere furnace, glasses were

Table 1 Summary of all starting materials, and data reported, in this study

Starting material			Data reported in this paper			
Composition	Synthesis	Form	XRD	Raman	CaPv stability	Decompression
$CaSiO_3$	1150 °C	Wollastonite			x	
$CaSiO_3$	Hot pressed at 7 GPa	Breyite				x
$CaSiO_3$ + 2 wt% H_2O	$CaSiO_3 + Ca(OH)_2 + SiO_2$	N/A			x	
$CaTiO_3$	1150 °C	Perovskite	x	x		
$Ca(Si_{0.52}Ti_{0.48})O_3$	$CaSiO_3 + CaTiO_3$, hot-pressed at 15 GPa	2 × CaPv	x	x		
$Ca(Si_{0.56}Ti_{0.44})O_3$	Fused at 1650 °C, hot-pressed at 15 GPa	CaPv	x	x		
$Ca(Si_{0.65}Ti_{0.35})O_3$	Fused at 1600 °C, hot-pressed at 15 GPa	CaPv	x	x		
$Ca(Si_{0.76}Ti_{0.24})O_3$*	Fused at 1600 °C, hot-pressed at 15 GPa	CaPv	x	x		x

checked for homogeneity, and ground to fine powders for use in experiments. Instead of being fused to a glass the $CaTiO_3$ and $CaSiO_3$ endmembers were sintered to form crystalline perovskite or wollastonite respectively. Crystallography of these endmember compositions was confirmed using a PANalytical X'Pert Pro powder diffractometer at UCL ($\lambda = 1.78897$ Å). A starting material composition with $x = 0.5$ (which could not be successfully quenched to a glass at 1 atmosphere) was formed by mixing $CaTiO_3$ and $CaSiO_3$ endmembers in appropriate proportions. Additionally a hydrous $CaSiO_3$ starting material was created by mixing the synthetic wollastonite with $Ca(OH)_2$ and SiO_2 in appropriate proportions to create a bulk composition equivalent to $CaSiO_3$ + 2 wt.% H_2O.

Samples used for ultrasonic experiments were hot-pressed to form the fully dense aggregates required for acoustic measurements. Ti-bearing CaPv samples were synthesised from glass starting materials by sintering at ~ 15 GPa and 1400 °C using a 10/5 multi anvil assembly at UCL. $Ca[Si_xTi_{1-x}]O_3$ samples, aside from that with $x = 0.5$, were visually inspected and believed to have fully converted to homogenous CaPv (this was confirmed by subsequent X-ray diffraction). As extremities of the $x = 0.5$ sample appeared to consist of two phases suggesting incomplete homogenisation (later confirmed by XRD) this sample was not used in ultrasonic experiments, however XRD and Raman data from the centre of this sample are presented. Finally, since perovskite-structured $CaSiO_3$ is experimentally unrecoverable to ambient conditions (Ringwood et al. 1971; Liu et al. 1975; Wang et al. 1994), synthetic wollastonite powder was hot-pressed into polycrystalline sample of breyite, the highest-pressure recoverable $CaSiO_3$ polymorph, at ~ 7 GPa and 1300 °C. The sintered starting materials with $x = 0.56$ and 1 are the same as those used by Thomson et al. (2019) (the sample labelled $x = 0.56$ was previously reported as $x = 0.6$). The reported chemical compositions of ultrasonic samples were determined after recovery from high pressure experiments via electron probe microanalysis.

Synchrotron diffraction experiments and Raman spectroscopy

X-ray diffraction patterns and Raman spectra of synthesised Ti-bearing CaPv samples were collected at ambient conditions prior to ultrasonic experiments. Diffraction patterns were collected on ID06-LVP ($\lambda = 0.22542$ or 0.3757 Å) over 360° azimuthal range using the standard Detection Technology detector available at the beamline (Guignard and Crichton 2015). Sample-detector distance was calibrated using a small aliquot of NIST LaB_6 660a standard powder positioned immediately adjacent to each sample. Raman spectra of these samples were collected using the off-line 532nm Raman spectrometer housed at beamline ID15B of the ERSF.

High-pressure experiments were performed at beamline ID06-LVP of the ESRF using 10/5 experimental assemblies consisting of Cr- or Co-doped MgO octahedra with ZrO_2 insulation surrounding MgO and Al_2O_3 inner parts. C-type W:Re thermocouples, with hot-junctions adjacent to samples, were used to monitor temperatures generated by graphite or TiB_2:BN heaters. Powdered starting materials (for phase relation experiments) were wrapped in Ni foil capsules, whilst pre-sintered samples (for acoustic measurements) were placed directly into an MgO sleeve. Pressure in experiments was monitored using the measured volumes of MgO, NaCl or Au and applying cross-calibrated equations of state (Dorogokupets et al. 2007).

In all experiments amorphous SiBCN(O) windows were inserted along the X-ray path to allow collection of high-quality angle-dispersive diffraction patterns from the samples using monochromatic X-rays ($\lambda = 0.2296$ or 0.22542 Å). Throughout the experiments both the standard Detection Technology X-scan 1D detector available on ID06-LVP (Guignard and Crichton 2015) and a Pixirad-8 detector were used. Data constraining the stability of $CaSiO_3$ were collected using the Pixirad-8 detector at ~ 5 s intervals. Alternatively, diffraction patterns collected during ultrasonic-type experiments, used in this study to investigate the decompression behaviour of CaPv minerals with $x = 0.76$ (unique to this study) and 1 (previously reported by Thomson et al. 2019), were collected using the Detection Technology X-scan detector. All sample-detector geometries were calibrated using a LaB_6 NIST 660a standard mounted in the sample position. Diffraction patterns were reduced and integrated using the Fit2 d software (Hammersley et al. 1997). Rietveld refinement of selected diffraction patterns were achieved using the GSAS software package (Larson et al. 1994).

Results

Ambient pressure crystal structure of $Ca[Si_xTi_{x-1}]O_3$ perovskites

Integrated 2-D diffraction patterns of $Ca[Si_xTi_{1-x}]O_3$ with $x = 0$, 0.52, 0.56, 0.65 and 0.76 collected at ambient conditions at UCL ($CaTiO_3$ only) and ID06-LVP are plotted in Fig. 1. Samples with $x = 0$, 0.56 and 0.65 are single phase, crystalline samples of perovskite; each has been refined in the *Pbnm* space group (lattice parameters reported in Table 2). The sample nominally with $x = 0.5$ is observed to consist of two coexisting perovskites with differing compositions (one that is approximately $Ca[Si_{0.52}Ti_{0.48}]O_3$ and a second that is close to possessing a $CaTiO_3$ composition)

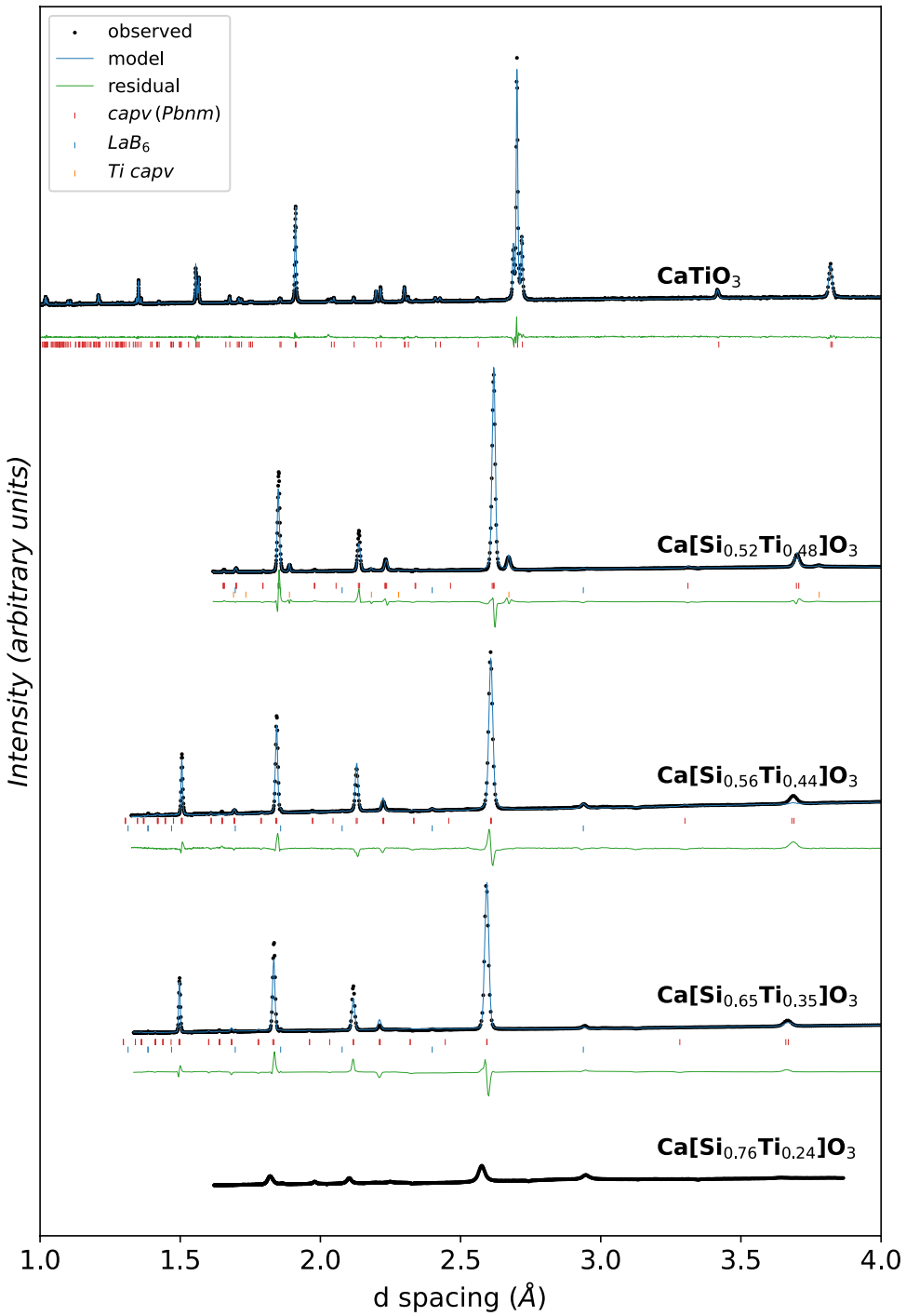

Fig. 1 Rietveld refined powder diffraction patterns of synthetic CaPv samples of variable composition as described in the text. Plotted as diffraction intensity vs. d-spacing. Black points are observed data, blue curve is the fitted model, green curve is the residual (unfitted) intensity and coloured ticks show the position of peaks from each phase. Diffraction was collected with the sample mounted immediately adjacent to LaB_6 powder as an independent calibration standard

reflecting the incomplete homogenisation of this sample. Diffraction patterns for this sample were refined using two $Ca[Si_xTi_{1-x}]O_3$ perovskite components. The sample with $Ca[Si_{0.76}Ti_{0.24}]O_3$ composition, instead of possessing sharp diffraction peaks, has a diffraction pattern consisting of weaker broad reflections. This is believed to reflect the partially amorphous nature of this sample and prevented refinement of this data. Instead, the d-spacings of the most prominent peaks were used to estimate an approximate pseudo-cubic lattice parameter for this sample.

Raman spectra of $Ca[Si_xTi_{x-1}]O_3$ perovskites

Raman spectra for $Ca[Si_xTi_{1-x}]O_3$ perovskite samples with $x = 0.52$, 0.56, 0.65 and 0.76 are plotted as the wavenumber shift relative to the 532 nm excitation laser in Fig. 2.

Table 2 Refined lattice parameters and volume of CaPv samples measured at ambient conditions in this study

CaPv composition	x	Refined space group	Incident X-ray λ (Å)	a (Å)	±	b (Å)	±	c (Å)	±	V (Å^3)	±
$CaTiO_3$	0	*Pbnm*	1.78897	5.381027	0.000088	5.441251	0.000094	7.641830	0.000123	223.749	0.010
$Ca(Si_{0.52}Ti_{0.48})O_3$	0.52	*Pbnm*	0.3757	5.235395	0.001410	5.239308	0.001353	7.389506	0.000458	202.693	0.007
$Ca(Si_{0.56}Ti_{0.44})O_3$	0.56	*Pbnm*	0.22542	5.219993	0.001035	5.214491	0.000779	7.363653	0.000817	200.435	0.010
$Ca(Si_{0.65}Ti_{0.35})O_3$	0.65	*Pbnm*	0.22542	5.187315	0.003173	5.190237	0.002933	7.320335	0.001078	197.088	0.015
$Ca(Si_{0.76}Ti_{0.24})O_3$*	0.76	$Pm\bar{3}\,m$	0.3757	3.64	*0.01*					48.3	*0.2*

*pseudo-cubic lattice estimated from d-spacing of peaks with illustrative uncertainty

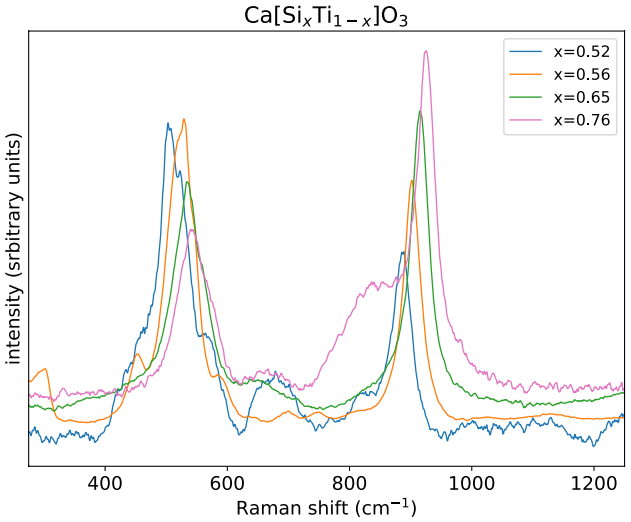

Fig. 2 Raman spectra of synthetic CaPv samples of variable composition in the interval 300–1200 cm^{-1}

For the x = 0.52 sample care was taken to ensure Raman spectra were collected from a fully equilibrated central portion of the sample. All Raman spectra are dominated by two major peaks, at 510–540 (labelled peak B1) and 880–894 cm^{-1} (peak A) (Fig. 2), which shift as the sample composition varies. In spectra of Ti–rich samples, especially those from previous studies, there is an additional peak (labelled B2) observed at slightly lower wavenumber than peak B1. Measured spectra from this study were baseline corrected and peak positions, which are reported in Table 3, were extracted by fitting Voigt peaks to the data using OriginPro. No temperature, or other, corrections were performed. Raman shifts corresponding to the same peaks for more Ti–rich perovskite samples, reported by Leinenweber et al. (1997), are also provided in Table 3.

Low-pressure stability limit of $CaSiO_3$ perovskite

Three experiments directly investigating the low-pressure stability field of $CaSiO_3$ perovskite were performed using powdered starting materials wrapped in Ni foil capsules. All three experiments were compressed at room temperature prior to heating to investigate phase relations at high *PT* conditions. Two experiments used a starting material of pure $CaSiO_3$ whereas one was performed in the presence of ~ 2 wt.% H_2O. The observations from all three of these experiments are summarised in Fig. 3, with a stack of the 1D integrated data from the water bearing experiment provided in Supplementary Fig. 1.

Table 3 Observed positions of dominant Raman peaks in CaPv samples from this, and previous, studies as a function of CaPv composition

$Ca(Si_xTi_{1-x})O_3$ composition (x)	source	A (cm^{-1})	B1 (cm^{-1})	B2 (cm^{-1})
0	This study	776.2	493.8	469.1
0.52	This study	888.9	532.2	506.2
0.56	This study	904.4	527.0	–
0.65	This study	917.4	538.2	–
0.76	This study	927.8	546.5	–
0	Leinenweber et al. 1997	*782.2*	*500.9*	*466.9*
0.05	Leinenweber et al. 1997	*778.8*	*498.3*	*470.3*
0.15	Leinenweber et al. 1997	*794.2*	*512.5*	*481.6*
0.25	Leinenweber et al. 1997	*824.9*	*502.9*	*470.1*
0.35	Leinenweber et al. 1997	*838.2*	*505.9*	*477.3*
0.5	Leinenweber et al. 1997	*898.2*	*520.9*	*480.7*
0.6	Thomson et al. 2016	*891*	*524*	–

Data in italics are re-reported from previous publications as indicated

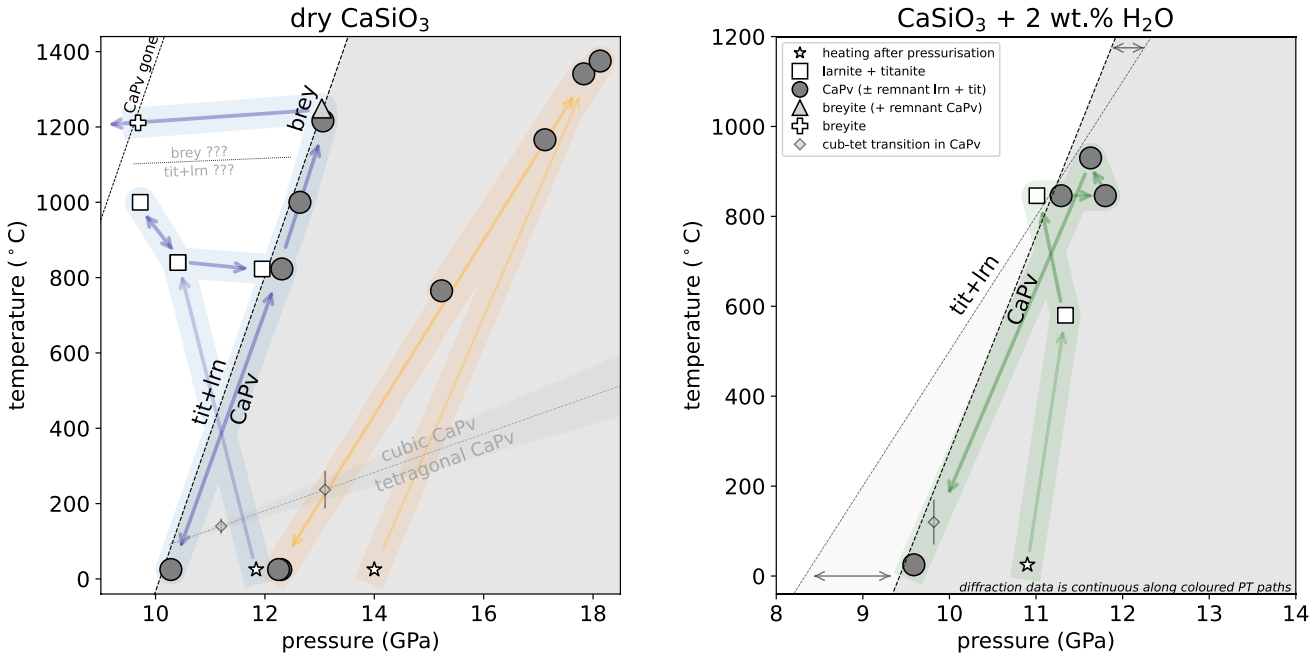

Fig. 3 PT summary of experiments conducted to investigate the low-pressure stability of $CaSiO_3$ perovskite, in **a** dry experiments and **b** experiments containing 2 wt% H2O within their bulk composition. Coloured arrows document experimental PT pathways, with symbols reflecting observed phase assemblages at specific conditions. Dashed lines plot suggested phase boundaries, which are based on the constraints from within experiments from this study as well as via comparison with Clapeyron slopes observed in previous works

Anhydrous experiments

In the initial anhydrous experiment, starting from a pressure of ~ 12 GPa the sample was incrementally heated over a period of several minutes. Diffraction peaks from the sample and cell components were observed to sharpen at ~ 850 °C and ~ 10.5 GPa. At these conditions the sample crystallised as a two-phase assemblage of titanite + larnite. The low crystallographic symmetry of both these phases prevents the conclusive indexing and full unit cell refinement for titanite and larnite using this experimental setup. Upon subsequent compression to increase the sample pressure at roughly constant temperature CaPv was observed to enter the phase assemblage, growing at the expense of titanite + larnite at pressures above ~ 12.3 GPa and 820 °C. Throughout this period of CaPv growth the sample pressure, as monitored by the diffraction of MgO (Dorogokupets et al. 2007), stopped increasing, presumably because

the ongoing titanite + larnite = CaPv reaction acted to buffer sample pressure. After significant CaPv growth the sample (which remained a three-phase assemblage as it still contained minor quantities of unreacted titanite + larnite) was cooled/reheated to/from room temperature. During cooling and reheating several of the diffraction peaks from either larnite or titanite underwent splitting, indicating a reversible phase transition in one of these materials had occurred. Upon reheating no change in the intensity of CaPv sample peaks was observed until ~ 1250 °C and 13.0 GPa when the intensity of CaPv started diminishing, whilst almost simultaneously all diffraction peaks corresponding to titanite + larnite were replaced by those indexing as breyite (the *PT* path associated with this cooling and heating can be observed in Fig. 3). This has been interpreted as the conditions of the CaPv out boundary into a low-pressure field of breyite stability. Breyite and CaPv coexisted during decompression at 1200–1250 °C until ~ 9.7 GPa, when the final CaPv diffraction peaks disappeared.

A second anhydrous experiment was compressed at room temperature to a higher initial pressure of ~ 14 GPa. In this experiment, single phase CaPv was observed to crystallise directly from the starting material upon heating at ~ 17.1 GPa and 1170 °C. Repeated heating/cooling ramps at constant press load between 12.25 GPa/25 °C and 18.1 GPa/1375 °C did not cross any dissociation reactions of CaPv. However, evidence for crossing the tetragonal-cubic transition in CaPv, identified by non-linear broadening of CaPv lattice reflections with temperature, were observed to occur at a temperature of 240 ± 50 °C (supplementary Fig. 1). Encroachment of the mica sheets, used as electrical insolation and lubrication on the back of the second-stage anvils, into the beam path caused diffraction patterns to be contaminated with several weak peaks that make Rietveld refinements and more precise identification of the transition temperature unfeasible.

H_2O bearing experiment

After initial room temperature compression to ~ 11 GPa, slow heating of the water-bearing starting material caused the diffraction peaks from cell components to sharpen as the sample crystallised between 580–620 °C and ~ 11.5 GPa, presumably in response to $Ca(OH)_2$ breakdown. On continued heating from this condition the sample pressure decreased until at 840 °C and 11 GPa diffraction peaks corresponded to a mixture of titanite and larnite. Sample pressure was increased whilst an approximately constant temperature was maintained until the CaPv in phase boundary was encountered. CaPv was observed to enter the phase assemblage at 11.3 GPa and 840 °C, identified by the growth of CaPv peaks at the expense of those from titanite + larnite. The appearance of CaPv occurred at ~ 1 GPa lower pressure than observed in the anhydrous experiment. Subsequently, despite continuing to increase the ram-pressure the sample pressure ceased increasing; it was again assumed pressure was buffered by the volume reduction associated with CaPv formation. Increasing temperature to 925 °C did not remove the remnant titanite + larnite from the phase assemblage. The sample was slowly cooled to room temperature. During cooling a phase transition was observed in one of the low-pressure phases, identified by splitting of several diffraction peaks at approximately 600 °C. Further discussion of this phase transition requires additional experimental investigation in a future study. From room temperature and 10 GPa the sample was recovered to ambient pressure.

Amorphisation of $CaSiO_3$ and $Ca[Si_{0.76}Ti_{0.24}]O_3$ perovskite

As already indicated, it has been previously established that $CaSiO_3$ undergoes amorphisation during decompression from high pressure conditions (Ringwood et al. 1971, Liu et al. 1975, Wang et al. 1994). The ability of ID06-LVP to collect continuous diffraction, in this case at least every 32 s throughout decompression allowed for this behaviour to be observed in more detail than achieved by previous studies.

Throughout decompression from ~ 12 GPa, following completion of ultrasonic measurements presented in Thomson et al. (2019), the volume evolution of an anhydrous $CaSiO_3$ perovskite sample at room temperature was monitored. Whilst the sample was initially observed to increase in crystallographic volume as pressure reduced, at pressures below ~ 4 GPa the behaviour of the $CaSiO_3$ sample deviated from its expected onward evolution. Instead of continuing to increase, the volume of CaPv apparently reduced with pressure from 4 GPa until the automated pressure release ramp, as controlled by the LVP software, was completed at approximately 1.5 GPa (Fig. 4b). This phenomenon of the crystallographic volume shrinking with decreasing pressure can be observed in the unrefined diffraction data (Fig. 4a) as a kink in the evolution of CaPv diffraction peaks (marked with red circles) towards higher 2θ at ~ 1–4 GPa whilst the diffraction peaks for other components (e.g. NaCl – yellow circles) continue to move towards smaller 2θ. It can also be observed that the maximum intensity of diffraction peaks from the CaPv reduce across the pressure interval from 3 to 1.5 GPa (Fig. 4a), possibly reflecting a decrease in the crystallinity of the sample. At this stage, although decompression was "complete", the press remained closed, and the sample continued to experience a remnant pressure of approximately 1–1.5 GPa. Under these conditions the sample remained partially crystalline, with its perovskite structure indicated by the continued presence of weak peaks indexable to the CaPv lattice. The press was subsequently opened whilst continuous 0.1 s diffraction patterns were collected (read out at 3.2 s

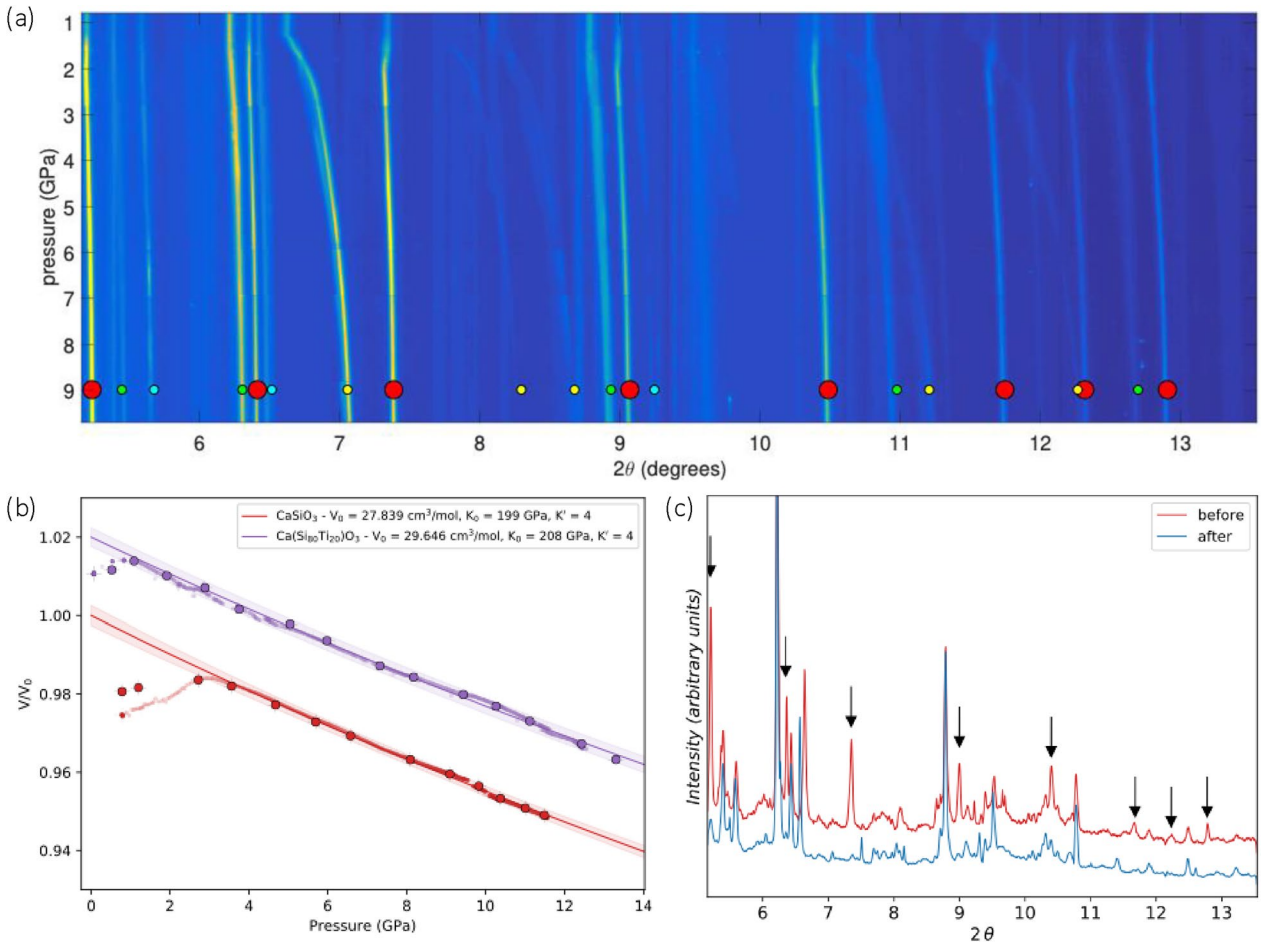

Fig. 4 **a** Diffraction from $CaSiO_3$ sample throughout room temperature decompression as a function of pressure, with colour intensity indicating the diffraction intensity. The peaks corresponding to $CaSiO_3$ are indicated with red dots, NaCl = yellow dots, MgO = green dots and Au = blue dots. **b** Refined volume of $CaSiO_3$ (red) and $Ca[Si_{0.8}Ti_{0.2}]O_3$ (purple) perovskite as a function of pressure (large symbols are full Rietveld refinements, small symbols are quick unit cell volumes based on the position of 2 diffraction peaks) overlain on fitted room temperature equations of state with 95% confidence intervals. Data and equation of state for $Ca[Si_{0.8}Ti_{0.2}]O_3$ is offset by +2% to allow visualisation. **c** Integrated 2D diffraction patterns of $CaSiO_3$ immediately before and after pressure release during press opening, demonstrating the rapid amorphisation of the sample at room temperature in under 3.2 s. The position of $CaSiO_3$ peaks prior to press opening are indicated with downward arrows

intervals). As the remnant pressure was released all remaining CaPv diffraction peaks disappeared below background levels in a time interval shorter than two consecutive data collections (< < 3.2 s, Fig. 4c). This suggests the sample almost instantaneously amorphised upon pressure release to ambient conditions. The continued presence of peaks from other cell components makes it impossible to ascertain whether the $CaSiO_3$ sample became entirely amorphous or remained very weakly crystalline as low intensity peaks may be hidden behind the non-zero background.

Assuming the refined volumes of $CaSiO_3$ from 12–4 GPa were unaffected by the later amorphisation (Fig. 4b), a 2nd-order Birch Murnaghan equation of state describing the decompression of tetragonal structured $CaSiO_3$ was fitted. EoS parameters of $V_0 = 46.23 \pm 0.04$ Å^3, $K_{T0} = 198.9$ GPa and $K_0' = 4$ are recovered (this data and EoS fit were previously reported in supplementary tables 2 and 4 of Thomson et al. 2019).

Similar amorphisation behaviour, although delayed to lower pressure, was also observed during decompression of a $Ca[Si_{0.76}Ti_{0.24}]O_3$ perovskite sample. Similar to the end-member $CaSiO_3$, the volume of $Ca[Si_{0.76}Ti_{0.24}]O_3$ increased with decreasing pressure from ~ 13 GPa until it deviated from expected behaviour below ~ 1.5 GPa. In this case the recovered perovskite material did not become completely amorphous, instead appearing to retain some degree of crystallinity at ambient conditions. Similarly, partial crystallinity is observed in diffraction patterns collected from starting materials with the same composition that were synthesised 2–4 weeks previously (Fig. 1). These observations

qualitatively suggest that either, (i) the amorphisation process is kinetically inhibited at room temperature, and/or (ii) $Ca[Si_{0.76}Ti_{0.24}]O_3$ is very close to the most silica-rich CaPv composition that is recoverable at room temperature.

Discussion

Ambient crystallography and spectroscopy of $Ca[Si_xTi_{1-x}]O_3$ perovskites

Previous studies have established that the lattice parameters, lattice volume and Raman spectra of CaPv materials, at least in the interval from $0 < x < 0.65$, vary systematically across the $CaTiO_3$-$CaSiO_3$ perovskite solid solution (Leinenweber et al. 1997, Leinenweber et al. 1997b, Kubo et al. 1997). As reconfirmed in this study, the $CaTiO_3$ endmember possesses an orthorhombic lattice (space group *Pbnm*) at ambient conditions (e.g. Knight et al. 2011) with pseudo-cubic lattice parameters $b' > c' > a'$ (where $a' = a/\sqrt{2}$, $b' = b/\sqrt{2}$ and $c' = c/2$). Increasing concentrations of the $CaSiO_3$ component in the $CaTiO_3$-rich half of the solid solution are known from previous studies to cause the lattice distortion to decrease towards an aristotype cubic perovskite lattice (Leinenweber et al. 1997; Kubo et al. 1997). Leinenweber et al. (1997b) reported a sample of the midway composition, Ca_2SiTiO_6 that appeared to possess a double-sized perovskite unit cell with cubic $Fm\bar{3}m$ symmetry displaying a 1:1 B-cation ordering scheme. In contrast, previous studies provide relatively few constraints on the crystal structure of more Si-rich CaPv compositions as there are only limited samples with reported compositions up to $Ca[Si_{0.65}Ti_{0.35}]O_3$. However, the composition of these most Si-rich CaPv's were not directly measured and were instead inferred from an extrapolation based on XRD-determined volumes (Kubo et al. 1997). Additionally, XRD data for these samples have poor counting statistics such that their utility beyond inferring the pseudo-cubic lattice parameters is limited. Thus, these data cannot independently confirm the effect of composition on CaPv volume.

Combining data from this study, refined assuming the *Pbnm* space group, with data from previous studies where either both chemistry and lattice parameters were directly measured or single-phase perovskites were synthesised from homogenous starting mixes, the linear evolution of volume across the entire CaPv solid solution is confirmed (as suggested by Ringwood et al., 1971; Leinenweber et al. 1997; Kubo et al. 1997). Compositions with $x \gtrsim 0.76$ are unrecoverable to ambient conditions (as observed by Ringwood et al. 1971). Thus, to extend comparisons to the $CaSiO_3$ endmember estimates of V_0 from equations of state (this study and Thomson et al. 2019) are plotted on Fig. 5.

Figure 5 demonstrates that the $CaSiO_3$ endmember should be almost 20% smaller than $CaTiO_3$ perovskite at ambient conditions. Shifting from $CaTiO_3$ endmember towards more Si-rich compositions it is observed that the octahedral distortion reduces, and the size order of the pseudo-cubic lattice parameters changes to $a' > b' > c'$ in the $CaSiO_3$-rich half of the solid solution. Regressing the

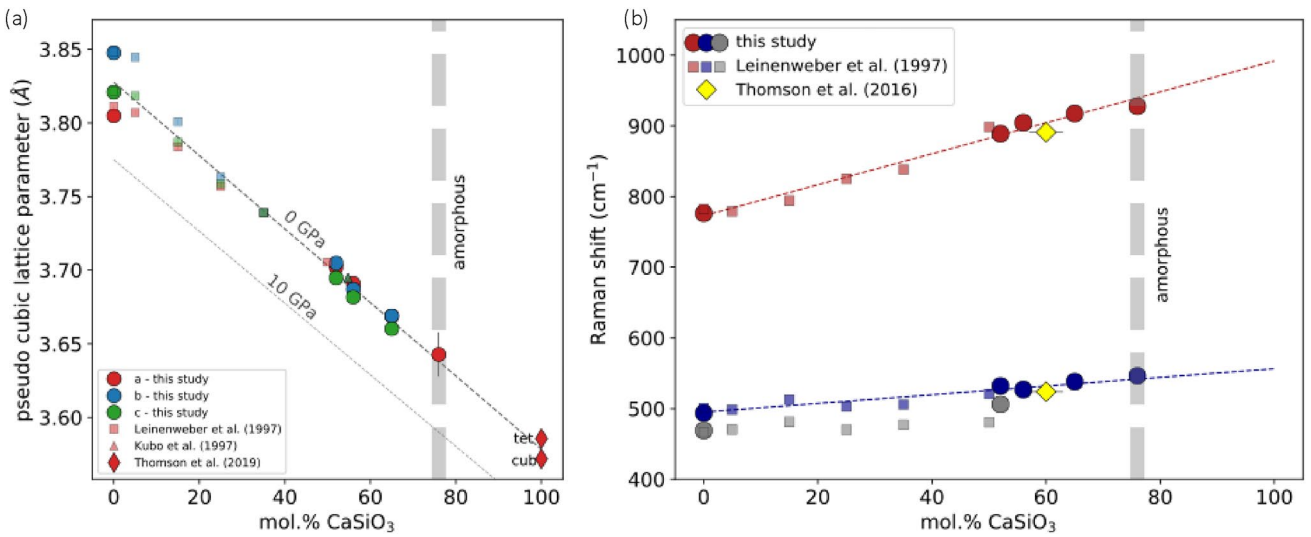

Fig. 5 **a** The evolution of CaPv pseudo-cubic lattice parameters as a function of CaPv composition. Black dashed curves plot a linear fit to the pseudo-cubic lattice parameter across all plotted data. The pale dashed line joins the volume of $CaTiO_3$ (Ross et al. 1999) and $CaSiO_3$ (Thomson et al. 2019) CaPv at 10 GPa, indicating the effect of pressure on unit cell volumes. **b** The evolution of CaPv's Raman peak positions with variable CaPv composition. Dashed lines plot linear fits as described in the text. Symbols and colours in (**a**) and (**b**) are defined in plot legends

pseudo-cubic lattice parameter of CaPv against composition provides the relationship a'(Å) = 3.82479–0.00240x (where x is the $CaSiO_3$ component in mol.%). In comparison with the effect of composition the volume change associated with 10 GPa of room temperature compression, calculated with the published equations of state of $CaSiO_3$ or $CaTiO_3$ (Ross et al., 1999; Thomson et al. 2019), is indicated as a dashed curve.

Coupled with the chemically induced crystallographic volume changes are equivalent shifts of the two (or three) dominant Raman modes of $Ca[Si_xTi_{1-x}]O_3$ perovskite. As identified above, the main features of Raman spectra of Si-rich perovskites are two modes found at 770–900 (peak A) and 490–550 (peak B1) cm^{-1}. When combined with spectra for Ti–rich CaPv compositions reported by Leinenweber et al. (1997), it is observed that these peaks evolve almost linearly across the entire $CaTiO_3$-$CaSiO_3$ perovskite solid solution. Fitting the observed peak positions to linear composition-frequency relationships ($f = aX + b$, where f is in cm^{-1} and X is the fraction of $CaSiO_3$ component in mol.%) a = 2.19 or 0.61 and b = 772.8 or 495.1 for the A and B1 frequency Raman modes respectively. Raman peak shifts observed from a synthetic CaPv mineral possessing a complex "natural" composition reported by Thomson et al. (2016), which ignoring minor components has the composition $Ca[Si_{0.6}Ti_{0.4}]O_3$, are plotted on Fig. 5b as yellow diamonds. This is in good agreement with peak systematics derived in this study, suggesting these features of Raman spectra are not largely affected by the presence of minor elements.

Based on the observed XRD and Raman systematics it should be possible to verify the mineralogy of candidate perovskite materials, such as diamond-hosted inclusions, without requiring the material to be at atmospheric conditions for chemical analyses. Combining measurement of XRD-derived volumes and the assumption that remnant inclusion pressures are limited to < 5 GPa, inclusion compositions can be estimated to better than ± 10 mol.% $CaSiO_3$. Similar estimates using Raman spectroscopy may be made, although because the pressure effect on peak shifts remains unquantified the accuracy of using a spectroscopy-only approach is currently unknown. Studying unexposed inclusions using a combination of X-ray diffraction and Raman spectroscopy can provide a tool for the identification of primary CaPv inclusions without risking amorphisation or loss during future studies. Alternatively, these systematics may also be used to constrain the composition of exsolved $CaTiO_3$ components in retrograded polyphase inclusions, allowing their bulk chemistry and/or pressure of re-equilibration to be estimated.

Low-pressure extent of $CaSiO_3$ perovskite stability

Previous estimates of the low-pressure extent of CaPv's stability field have used quench-based multi-anvil cell (Akaogi et al. 2004; Gasparik et al. 1994), *in-situ* multi-anvil (Wang et al. 1994; Sueda et al. 2006) and *in-situ* diamond anvil cell approaches (Shim et al. 2000). However, comparison of results from these studies reveals significant variability; the low-pressure extent of CaPv stability ranges from 11 to 16 GPa at 1200 °C (Fig. 6). These variations may, at least partly, be explained by (i) the large volume change (> 30%) required to transform experimental starting materials to CaPv which will drastically reduce the accuracy of pressure calibrations in quench experiments (Akaogi et al. 2004; Gasparik et al. 1994) and (ii) the use of different pressure markers in *in-situ* studies. Additionally, our results now also imply that (iii) the presence of H_2O in the sample environment alters the extent of the CaPv stability field. It is challenging to evaluate the extent to which each of these three factors may have affected previous studies, but we are aware that at least one previous study (Gasparik et al. 1994) deliberately introduced water to promote reaction kinetics. Generally, in high-pressure experiments it is not uncommon for small quantities of water vapour, whether accidentally or deliberately, to be included in samples. Indeed, whilst we report results from anhydrous and hydrous experiments, we do not and cannot verify that anhydrous runs were entirely free from water. Anhydrous experiments were prepared from dried starting materials and baked experimental components; however, trace amounts of water were most likely present in the experiments. The true increase in CaPv's breakdown pressure in completely anhydrous experiments may therefore be larger than observed in this study. Additionally, we are fairly certain that the Ni capsules used in this study would not prevent the escape of free-water at run conditions, such that we only interpret our hydrous experiments as having some quantity of water present. Beyond the individual study of Gasparik et al. (1994) it is also impossible to conjecture on whether water's presence explains the discrepancies between other published studies. We instead focus only on the observations made in this study, plotting our results alongside previous studies to facilitate readers' comparisons (Fig. 6).

Observations from our experiments performed with and without H_2O presence, but that were otherwise identical, directly imply that water extends the CaPv stability field to at least 1 GPa lower pressure. The unit cell volume measurements of MgO, which are used as a pressure standard via the equations of state of Dorogokupets et al. (2007) in this study, are sufficiently precise that quantifiable pressure uncertainties are < 0.1 GPa. This precision is far smaller than the observed pressure difference between the CaPv appearance with and without H_2O (~ 1 GPa at ~ 800 °C).

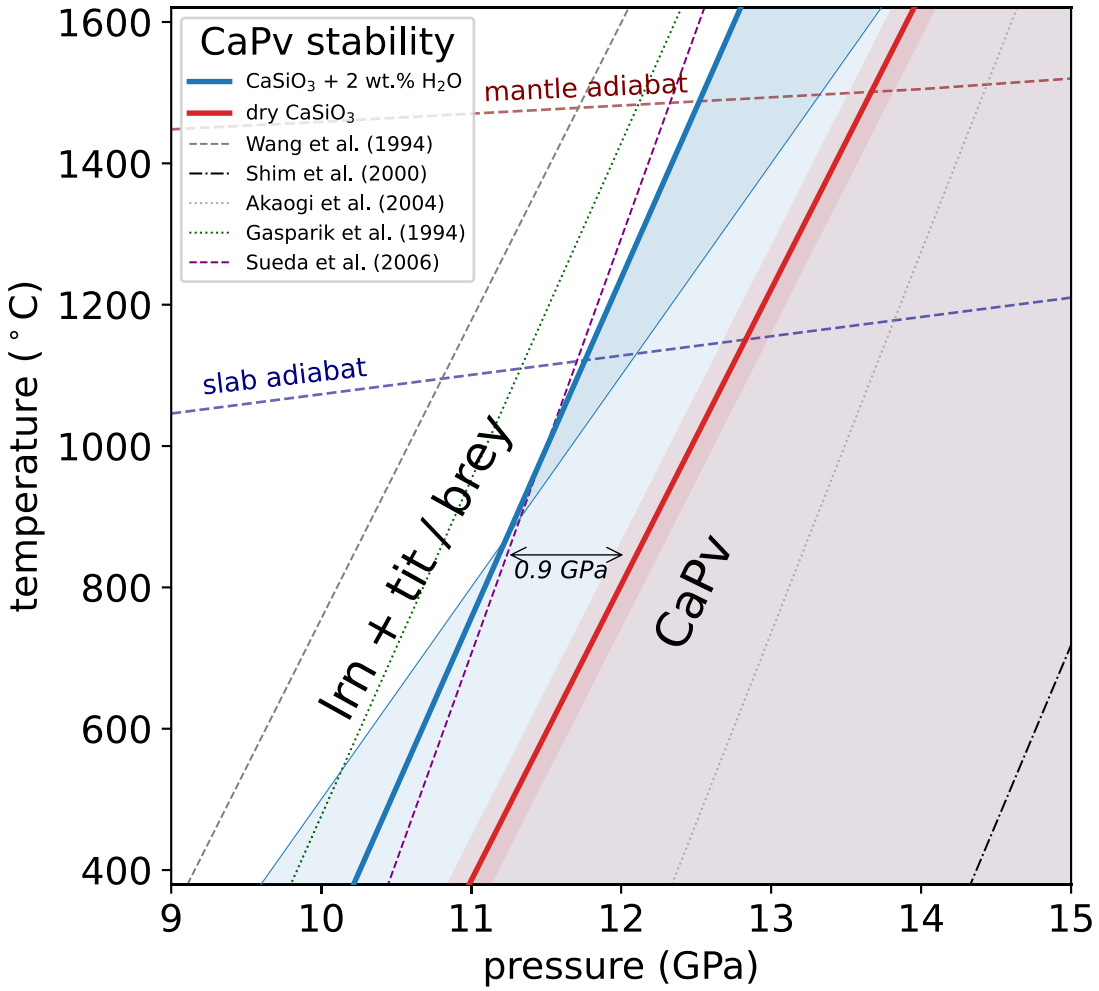

Fig. 6 Summary of the conditions of CaPv stability in PT space under "dry" and "wet" conditions compared with previous studies. Blue and red dashed lines represent a typical slab adiabat and mantle adiabatic temperature profile

One explanation for this observation is that CaPv incorporates sufficient water in its crystal structure to stabilise CaPv to lower pressure. This implication is consistent with recent experimental results suggesting water incorporation alters the crystal symmetry of CaPv at high *PT* conditions (Chen et al. 2020). Alternatively, the presence of water could be acting as a catalyst to increase reaction kinetics, reducing the pressure overstep required for CaPv growth. However, rapid occurrence of all observed reactions in this study (seconds to minutes) suggest that sluggish kinetics alone are unlikely to explain this difference. Instead, these observations imply water expands the field of CaPv stability, although further investigations of this effect should be undertaken for an improved understanding.

Observations from this study place the appearance of $CaSiO_3$ perovskite between previous pressure estimates (Fig. 6) (Akaogi et al. 2004; Gasparik et al. 1994; Wang et al. 1994; Sueda et al. 2006; Shim et al. 2000). At adiabatic mantle temperatures experiments from this study predict that CaPv (with a pure $CaSiO_3$ composition) becomes stable at ~ 13.5 GPa (~ 400 km depth), compared with ~ 12.5 GPa at temperature conditions of a subducting slab (~ 380 km depth). The presence of water appears to expand this stability field by at least ~ 1 GPa towards lower pressure (~ 30 km).

Additionally, of interest from these experiments, we note that the direct conversion of CaPv to breyite on decompression (at ~ 1250 °C and ~ 12.5 GPa) was observed without an intermediate stability field of titanite + larnite. This differs from the results of all previous studies, however current observations remain insufficient for a complete explanation such that we limit our insights to a few simple comments about our observations. This study utilised high-resolution monochromatic diffraction, which is particularly suited for discriminating between the low-symmetry mineral phases. Each of breyite (triclinic, Brenker et al. 2021), titanite (triclinic or monoclinic, Angel et al. 1997) and larnite (monoclinic, Xiong et al. 2016) and have relatively large unit

cells. Thus, all three phases possess many diffraction peaks at low 2θ angles, which can make it non-trivial to distinguish between them and certainly makes refinement of their unit cells challenging. Our experience demonstrated these issues, just as previous studies will have done. However, upon decompression from ~ 13 GPa and 1250 °C the appearance of breyite at the expense of titanite + larnite was definitively observed. Breyite coexisted with CaPv over a decompression interval of ~ 3 GPa until a single phase breyite assemblage existed below ~ 9.7 GPa. The extended cooccurrence of breyite and CaPv is believed to result from the large volume increase (~ 30%) required for this phase transition, and is not believed to result solely from sluggish kinetics. The full conversion of CaPv to breyite was completed in < 60 min at 1200 °C. This appearance of breyite, in place of larnite + titanite, occurred at significantly higher pressure compared with previous experiments, however, we are unaware of other studies collected data during high temperature decompression. Further insight into these observations is beyond the scope of this study.

Conclusions

Former CaPv inclusions in diamonds, consisting of breyite ± perovskite ± titanite ± larnite, are some of the most commonly observed in sub-lithospheric diamonds (Brenker et al. 2021). Retrograded CaPv inclusions have been reported in diamonds from from sources in Brazil (Brenker et al. 2007, Harte et al. 1994; 1999, Harte et al. Zedgenizov et al. 2014, Hayman et al. 2005, Kaminsky et al. 2001, Joswig et al. 1999, Thomson et al. 2014, Bulanova et al. 2010, Walter et al. 2008, Walter et al. 2011, Burnham et al. 2015, Zedgenizov et al. 2016, Anzolini et al. 2016, Anzolini et al. 2018, Smith et al. 2018) Kankan (Stachel et al. 2000; Brenker et al. 2005), Canada (Davies et al. 2004; Tappert et al. 2005) and Southern Africa (Korolev et al. 2018; Smith et al. 2018). In comparison there have only been two reports of inclusions of "primary" CaPv (Nestola et al. 2018; Tschauner et al. 2021). However, comparison of the unit cell volume and Raman spectra of the inclusion reported by Nestola et al (2018) with volume and Raman systematics from this study (Fig. 5) suggests it was likely misidentified and instead is a retrograde wollastonite + $CaTiO_3$ inclusion assemblage. Similarly, the inclusion described by Tschauner et al (2021), due to the reasoning presented by Walter et al. (2022), is not believed to be pristine CaPv although no Raman spectra of this inclusion is available for comparison with additional constraints from this study. We therefore remain unaware of any pristine $CaSiO_3$ perovskite inclusions. Given the rapid amorphisation observed during room temperature decompression we suggest a very specific *PT* exhumation pathway – which is yet to be sampled – may be required for preservation of this mineral type as a diamond-hosted inclusion.

The data presented in this study provides tools that can be used in future work to verify prospective CaPv inclusions using non-invasive X-ray diffraction and/or Raman spectroscopy. Additionally, these tools will also allow the chemistry of CaPv minerals, including those within retrograded inclusion assemblages, to be evaluated *in-situ*. Finally, our experiments demonstrate that the minimum pressure of $CaSiO_3$ perovskite stability appears to vary with water concentration, with CaPv potentially stable at pressures as low as ~ 11.5 GPa within subducting slabs.

Supplementary Information The online version contains supplementary material available at https://doi.org/10.1007/s00269-025-01321-z.

Author contribution A.T. designed the measurements within this study. All authors contributed to the experiments over multiple synchrotron beam time allocations. A.T., W.C. and J.B. wrote the main manuscript text. All authors contributed to discussions and reviewed the manuscript.

Funding The research leading to these results received funding from the UK Natural Environmental Research Council under Grant Agreement No. NE/P017657/1.

Data availability No datasets were generated or analysed during the current study.

Declarations

Conflict of interest The authors have no relevant financial or non-financial interests to disclose.

References

Akaogi M, Yano M, Tejima Y, Iijima M, Kojitani H (2004) High-pressure transitions of diopside and wollastonite: phase equilibria and thermochemistry of $CaMgSi_2O_6$, $CaSiO_3$ and $CaSi_2O_5$–$CaTiSiO_5$ system. Phys Earth Planet Inter 143:145–156

Angel RJ (1997) Transformation of fivefold-coordinated silicon to octahedral silicon in calcium silicate, $CaSi_2O_5$. Am Mineral: J Earth Planet Mater 82(7–8):836–839

Anzolini C, Angel RJ, Merlini M, Derzsi M, Tokár K, Milani S, Krebs MY, Brenker FE, Nestola F, Harris JW (2016) Depth of formation of $CaSiO_3$-walstromite included in super-deep diamonds. Lithos 265:138–147

Anzolini C, Prencipe M, Alvaro M, Romano C, Vona A, Lorenzon S, Smith EM, Brenker FE, Nestola F (2018) Depth of formation of super-deep diamonds: Raman barometry of $CaSiO_3$-walstromite inclusions. Am Miner 103(1):69–74

Brenker FE, Vincze L, Vekemans B, Nasdala L, Stachel T, Vollmer C, Kersten M, Somogyi A, Adams F, Joswig W, Harris JW (2005) Detection of a Ca-rich lithology in the Earth's deep (> 300 km) convecting mantle. Earth Planet Sci Lett 236(3–4):579–587

Brenker FE, Vollmer C, Vincze L, Vekemans B, Szymanski A, Janssens K, Szaloki I, Nasdala L, Joswig W, Kaminsky F (2007) Carbonates from the lower part of transition zone or even the lower mantle. Earth Planet Sci Lett 260(1–2):1–9

Brenker FE, Nestola F, Brenker L, Peruzzo L, Harris JW (2021) Origin, properties, and structure of breyite: the second most abundant mineral inclusion in super-deep diamonds. Am Miner 106(1):38–43

Bulanova GP, Walter MJ, Smith CB, Kohn SC, Armstrong LS, Blundy J, Gobbo L (2010) Mineral inclusions in sublithospheric diamonds from Collier 4 kimberlite pipe, Juina, Brazil: subducted protoliths, carbonated melts and primary kimberlite magmatism. Contrib Miner Petrol 160:489–510

Burnham AD, Thomson AR, Bulanova GP, Kohn SC, Smith CB, Walter MJ (2015) Stable isotope evidence for crustal recycling as recorded by superdeep diamonds. Earth Planet Sci Lett 432:374–380

Chen H, Leinenweber K, Prakapenka V, Prescher C, Meng Y, Bechtel H, Kunz M (2020) Possible H_2O storage in the crystal structure of $CaSiO_3$ perovskite. Phys Earth Planet Inter 299:106412

Davies RM, Griffin WL, O'Reilly SY, Doyle BJ (2004) Mineral inclusions and geochemical characteristics of microdiamonds from the DO27, A154, A21, A418, DO18, DD17 and Ranch Lake kimberlites at Lac de Gras, Slave Craton. Canada Lithos 77(1–4):39–55

Dorogokupets PI, Dewaele A (2007) Equations of state of MgO, Au, Pt, NaCl-B1, and NaCl-B2: Internally consistent high-temperature pressure scales. High Pressure Research 27(4):431–446

Gasparik T, Wolf K, Smith CM (1994) Experimental determination of phase relations in the $CaSiO_3$ system from 8 to 15 GPa. Am Miner 79(11–12):1219–1222

Guignard J, Crichton WA (2015) The large volume press facility at ID06 beamline of the European synchrotron radiation facility as a High Pressure-High Temperature deformation apparatus. Rev Sci Instrum 86(8):085112

Hammersley AP (1997) FIT2D: an introduction and overview. Eur Synchrotron Radiat Facil Internal Rep 68:58

Harte B, Harris JW (1994) Lower mantle mineral associations preserved in diamonds. Mineral Mag A 58:384–385

Harte B (1999) Lower mantle mineral associations in diamonds from Sao Luiz, Brazil. Mantle petrology: Field observations and high-pressure experimentation: A tribute to Francis R. (Joe) Boyd 6:125–153

Hayman PC, Kopylova MG, Kaminsky FV (2005) Lower mantle diamonds from Rio Soriso (Juina area, Mato Grosso, Brazil). Contrib Miner Petrol 149:430–445

Holland TJ, Hudson NF, Powell R, Harte B (2013) New thermodynamic models and calculated phase equilibria in NCFMAS for basic and ultrabasic compositions through the transition zone into the uppermost lower mantle. J Petrol 54(9):1901–1920

Ishii T, Kojitani H, Akaogi M (2019) Phase relations of harzburgite and MORB up to the uppermost lower mantle conditions: precise comparison with pyrolite by multisample cell high-pressure experiments with implication to dynamics of subducted slabs. J Geophys Res: Solid Earth 124(4):3491–3507

Joswig W, Stachel T, Harris JW, Baur WH, Brey GP (1999) New Ca-silicate inclusions in diamonds—tracers from the lower mantle. Earth Planet Sci Lett 173(1–2):1–6

Kaminsky F, Zakharchenko O, Davies R, Griffin W, Khachatryan-Blinova G, Shiryaev A (2001) Superdeep diamonds from the Juina area, Mato Grosso state, Brazil. Contrib Miner Petrol 140:734–753

Kesson SE, Fitz Gerald JD, Shelley JM (1998) Mineralogy and dynamics of a pyrolite lower mantle. Nature 393(6682):252–255

Knight KS (2011) Structural and thermoelastic properties of $CaTiO_3$ perovskite between 7 K and 400 K. J Alloy Compd 509(22):6337–6345

Ko, B., Greenberg, E., Prakapenka, V., Alp, E. E., Bi, W., Meng, Y., ... & Shim, S. H. (2022). Calcium dissolution in bridgmanite in the Earth's deep mantle. *Nature*, *611*(7934), 88–92.

Korolev N, Kopylova M, Gurney JJ, Moore AE, Davidson J (2018) The origin of Type II diamonds as inferred from Cullinan mineral inclusions. Mineral Petrol 112:275–289

Kubo A, Suzuki T, Akaogi M (1997) High pressure phase equilibria in the system $CaTiO_3$-$CaSiO_3$: stability of perovskite solid solutions. Phys Chem Miner 24:488–494

Larson AC, Von Dreele RB (1994) GSAS. Report lAUR, 86–748

Leinenweber K, Parise J (1997) Rietveld refinement of Ca_2TiSiO_6 perovskite. Am Miner 82(5–6):475–478

Leinenweber K, Grzechnik A, Voorhees M, Navrotsky A, Yao N, McMillan PF (1997) Structural variation in $Ca(Ti_xSi_{1-x})O_3$ perovskites (1> x> 0.65) and the ordered phase Ca_2TiSiO_6. Phys Chem Miner 24:528–534

Liu LG, Ringwood AE (1975) Synthesis of a perovskite-type polymorph of $CaSiO_3$. Earth Planet Sci Lett 28(2):209–211

Muir JM, Thomson AR, Zhang F (2021) The miscibility of calcium silicate perovskite and bridgmanite: A single perovskite solid solution in hot, iron-rich regions. Earth Planet Sci Lett 566:116973

Nestola F, Korolev N, Kopylova M, Rotiroti N, Pearson DG, Pamato MG, Alvaro M, Peruzzo L, Gurney JJ, Moore AE, Davidson J (2018) $CaSiO_3$ perovskite in diamond indicates the recycling of oceanic crust into the lower mantle. Nature 555(7695):237–241

Ricolleau, A., Perrillat, J. P., Fiquet, G., Daniel, I., Matas, J., Addad, A., ... & Guignot, N. (2010). Phase relations and equation of state of a natural MORB: Implications for the density profile of subducted oceanic crust in the Earth's lower mantle. *Journal of Geophysical Research: Solid Earth*, 115(B8).

Ringwood AE, Major A (1971) Synthesis of majorite and other high pressure garnets and perovskites. Earth Planet Sci Lett 12(4):411–418

Ross NL, Angel RJ (1999) Compression of $CaTiO_3$ and $CaGeO_3$ perovskites. Am Miner 84(3):277–281

Shim SH, Duffy TS, Shen G (2000) The stability and P-V–T equation of state of $CaSiO_3$ perovskite in the Earth's lower mantle. J Geophys Res: Solid Earth 105(B11):25955–25968

Smith EM, Shirey SB, Richardson SH, Nestola F, Bullock ES, Wang J, Wang W (2018) Blue boron-bearing diamonds from Earth's lower mantle. Nature 560(7716):84–87

Stachel T, Harris JW, Brey GP, Joswig W (2000) Kankan diamonds (Guinea) II: lower mantle inclusion parageneses. Contrib Miner Petrol 140(1):16–27

Stixrude L, Lithgow-Bertelloni C (2012) Geophysics of chemical heterogeneity in the mantle. Annu Rev Earth Planet Sci 40:569–595

Sueda Y, Irifune T, Yamada A, Inoue T, Liu X, Funakoshi KI (2006) The phase boundary between $CaSiO_3$ perovskite and Ca_2SiO_4+ $CaSi_2O_5$ determined by in situ X-ray observations. Geophys Res Lett. https://doi.org/10.1029/2006GL025772

Tappert R, Stachel T, Harris JW, Muehlenbachs K, Ludwig T, Brey GP (2005) Diamonds from Jagersfontein (South Africa): messengers from the sublithospheric mantle. Contrib Miner Petrol 150:505–522

Thomson AR, Kohn SC, Bulanova GP, Smith CB, Araujo D, Walter MJ (2014) Origin of sub-lithospheric diamonds from the Juina-5

kimberlite (Brazil): constraints from carbon isotopes and inclusion compositions. Contrib Mineral Petrol 168:1–29

Thomson AR, Walter MJ, Kohn SC, Brooker RA (2016) Slab melting as a barrier to deep carbon subduction. Nature 529(7584):76–79

Thomson AR, Crichton WA, Brodholt JP, Wood IG, Siersch NC, Muir JMR, Dobson DP, Hunt SA (2019) Seismic velocities of $CaSiO_3$ perovskite can explain LLSVPs in Earth's lower mantle. Nature 572(7771):643–647

Tschauner O, Huang S, Yang S, Humayun M, Liu W, Gilbert Corder SN, Bechtel HA, Tischler J, Rossman GR (2021) Discovery of davemaoite, $CaSiO_3$-perovskite, as a mineral from the lower mantle. Science 374(6569):891–894

Walter MJ, Bulanova GP, Armstrong LS, Keshav S, Blundy JD, Gudfinnsson G, Lord OT, Lennie AR, Clark SM, Smith CB, Gobbo L (2008) Primary carbonatite melt from deeply subducted oceanic crust. Nature 454(7204):622–625

Walter MJ, Kohn SC, Araujo D, Bulanova GP, Smith CB, Gaillou E, Wang J, Steele A, Shirey SB (2011) Deep mantle cycling of oceanic crust: evidence from diamonds and their mineral inclusions. Science 334(6052):54–57

Walter MJ, Kohn SC, Pearson GD, Shirey SB, Speich L, Stachel T, Thomson AR, Yang J (2022) Comment on ", $CaSiO_3$-perovskite, as a mineral from the lower mantle." Science 376(6593):eabo2029

Wang Y, Weidner DJ (1994) Thermoelasticity of $CaSiO_3$ perovskite and implications for the lower mantle. Geophys Res Lett 21(10):895–898

Woodland AB, Girnis AV, Bulatov VK, Brey GP, Höfer HE (2020) Breyite inclusions in diamond: experimental evidence for possible dual origin. Eur J Mineral 32(1):171–185

Xiong Z, Liu X, Shieh SR, Wang S, Chang L, Tang J, Hong X, Zhang Z, Wang H (2016) Some thermodynamic properties of larnite (β-Ca_2SiO_4) constrained by high T/P experiment and/or theoretical simulation. Am Mineral. https://doi.org/10.2138/am-2016-5425

Zedgenizov DA, Kagi H, Shatsky VS, Ragozin AL (2014) Local variations of carbon isotope composition in diamonds from São-Luis (Brazil): evidence for heterogenous carbon reservoir in sublithospheric mantle. Chem Geol 363:114–124

Zedgenizov DA, Ragozin AL, Kalinina VV, Kagi H (2016) The mineralogy of Ca-rich inclusions in sublithospheric diamonds. Geochem Int 54:890–900